RSC Advances

PAPER

View Article Online
View Journal | View Issue

Cite this: *RSC Adv.*, 2015, **5**, 6932

A novel polyurethane/cellulose fibrous scaffold for cardiac tissue engineering

Po-Hsuen Chen,[a] Hsueh-Chung Liao,[b] Sheng-Hao Hsu,[c] Rung-Shu Chen,[d] Ming-Chung Wu,[e] Yi-Fan Yang,[f] Chau-Chung Wu,[g] Min-Huey Chen*[d] and Wei-Fang Su*[b]

Received 16th October 2014
Accepted 18th December 2014

DOI: 10.1039/c4ra12486c

www.rsc.org/advances

The present work demonstrates a biomimetic electrospun scaffold based on polyurethane (PU) and ethyl cellulose (EC), featuring uniform fibrous nanostructures and three dimensional porous networks. The relationship between processing conditions and fibrous nanostructures is established which guides the rational processing with tunable fiber diameters. Additionally, the developed scaffold template reveals biocompatibility in retention and proliferation of cardiac myoblast H9C2 cells. The high mechanical strength of the PU/EC scaffolds enables the processing and handling of an ultrathin patch. Their elastomeric characteristics revealed the compatibility between the patch and contractile tissues. Furthermore, anisotropic PU/EC scaffolds with aligned nanofibers were successfully fabricated, exhibiting higher mechanical strength and essential characteristics for the survival and function of cardiac cells with native anisotropy. This work demonstrates a bioengineered PU/EC fibrous scaffold with uniform nanostructural webs and provides insight into the relationships between processing control, nanostructures and associated properties, with promising potential in cardiac tissue engineering.

1 Introduction

Myocardial infarction is one of the leading causes of morbidity and mortality.[1] Tissue engineering which integrates porous template of scaffolds based on biomaterials and functional cells has been extensively explored and represents the most potentially feasible strategy for attaining therapeutic purposes.[1–4] During the past two decades, developing bioactive scaffold patches for mimicking the extracellular matrix of myocardium has become the major goal in order to regenerate and reconstruct damaged myocardium. The biomimetic scaffolds can be fabricated from either nature materials[5–9] (*e.g.* collagen, polysaccharide, alginate, *etc.*) or synthetic polymers[10–15] (*e.g.* poly(glycolic acid), poly(lactic acid), poly(*p*-dioxanone), poly(glycerol sebacate), polyurethane, *etc.*). Natural scaffold provides physiologically relevant template for cell retention, proliferation and differentiation; however, most of them are weak in durability and large variations among different isolated batches limit their practical applications *in vivo*.[15,16] In contrast, synthetic polymer possesses higher mechanical strength and thus improves the processibility and handling of ultra-thin scaffold patches. Moreover, the mechanical properties, scaffold nanostructures, chemical composition, *etc.* can be easily tailored to suit a variety of applications. Therefore, blends of synthetic materials and nature materials are promising in taking both advantages of biocompatibility and suitable mechanical properties.

The morphologies/structures of scaffolds are crucial in providing guidance cues for cellular regulation. Electrospinning process has attracted intensive investigations recently owing to its versatility in fabricating fibrous structures.[13–15,17–22] The high surface-area to volume ratio leads to the interconnected porous networks which assist in nutrition perfusion and diffusions. Additionally, fiber diameter in nanometer scale (1–1000 nm) can be achieved which resembles the architecture of natural cardiac extracellular matrices and thus facilitates cell retention, proliferation and differentiation. Most important of all, for the myocardial tissue with native anisotropic textures and functions, electrospinning enables aligned fibrillar structure that provides topographic cues for cell orientation.[23–27] Polyurethane is a promising elastomer with excellent mechanical properties for cardiac tissue engineering.[25,26,28–34] However, the scaffolds fabricated from electrospun polyurethane for cardiac tissue

[a]*Institute of Oral Biology, School of Dentistry, National Taiwan University, Taipei 10002, Taiwan*
[b]*Department of Materials Science and Engineering, National Taiwan University, Taipei 10617, Taiwan. E-mail: suwf@ntu.edu.tw*
[c]*Institute of Polymer Science and Engineering, National Taiwan University, Taipei 10617, Taiwan*
[d]*Graduate Institute of Clinical Dentistry, School of Dentistry, National Taiwan University, Taipei 10002, Taiwan. E-mail: minhueychen@ntu.edu.tw*
[e]*Department of Chemical and Materials Engineering, Chang Gung University, Taoyuan 33302, Taiwan*
[f]*Department of Internal Medicine, National Taiwan University Hospital, Taipei 10002, Taiwan*
[g]*Department of Primary Care Medicine, College of Medicine, National Taiwan University, Taipei 10002, Taiwan*

engineering usually reveals winding and relatively non-uniform nanofibers in diameter (or even with beads) with intertwining and clinginess among the nanofibers.[17,23,25,32,33,35] It would consequently limit the construction of three dimensional interconnecting porous structures thus deteriorate nutrients profusions and diffusions untaken by cardiomyocytes. Therefore, controlling the properties of polymer solutions toward high quality electrospun scaffolds with three dimensional webs/networks is crucial in the application of cardiac tissue engineering.

Polymer blend provides a promising strategy to tailor the properties of scaffolds. In the present work we demonstrate an electrospun fibrous scaffold which combines the advantages of both synthetic polymer polyurethane (PU) and nature polymer ethyl cellulose (EC). The relation between the nanofiber diameter and processing conditions of electrospinning was analytically correlated in terms of solution concentrations and electrospinning parameters. Additionally, to access the potential in engineered cardiac graft, we present the biocompatibility of the PU/EC scaffolds which were systematically investigated by cell proliferation, morphological/topographical observation and immunocytochemistry characterization. The mechanical properties of the PU/EC scaffolds were explored with respective to polymer blending ratios and nanofiber diameters. Furthermore, for structurally mimicking the anisotropic extracellular matrix (ECM) of native heart muscles, PU/EC scaffolds with aligned nanofibers were fabricated by employing a rotating collector for orientating the nanofibers. We compare the scaffold substrates with random and aligned nanofibers in the viability of cell retention/proliferation, mechanical properties, and cell guidance.

2 Materials and methods

2.1 Fabrication of PU/EC electrospun scaffolds

The PU (Elasturan T6100, BASF) and EC (ACROS) were purchased and used as received. Solvents: acetone (99.5%, ACROS), tetrahydrofuran (THF, 99.5%, ACROS) and dimethylacetamide (DMAc, 99.5%, ACROS) were used as received without further purification. After being immersed in acetone overnight, the PU was washed by DI-water and then dried in oven at 80 °C overnight. The PU/EC solutions in THF–DMAc co-solvent (2/3, v/v) with concentrations of 4 wt%, 6 wt%, 8 wt% and 10 wt% were prepared with respective to PU/EC blending ratios of 9/1, 4/1 and 1/1 (w/w). The pristine PU solution was also prepared as the control sample. All of the blending polymer solutions were stirred overnight for ensuring completely mixing. The scaffolds were fabricated by electrospinning using an apparatus consisting of a variable speed syringe pump (KDS-100, KD Scientific), a high voltage power supply (You Shang Technical Corp.), and a metal collector. A 3 ml syringe (Teruom, 24 gauge) was installed on the apparatus which continuously feed the polymer solutions with a flow rate of 0.5–1 ml h^{-1}. When a high voltage was applied, a solution drop on the needle tip was forced to become a "Taylor cone" and then ejected to the grounded collector to generate nanofibers. The isotropic nanofibers were collected by a metal plate with diameter of 20 cm which was rotating at 280 r.p.m whereas the aligned nanofibers were collected by a driving belt with a speed of 550 cm s^{-1}. Both types of collector were covered with aluminum sheets and located at fixed distances of 15 cm and 10 cm for isotropic and aligned nanofibers respectively. As-electrospun scaffolds were vacuumed overnight for removing residual solvent.

The denotation of electrospun PU/EC fibrous scaffolds is P*x*C*y*_diameter, with $x:y$ indicating the blending ratio of polyurethane (P) to cellulouse (C). The nanofiber diameter were controlled around 100 nm, 500 nm and 1000 nm which are denoted as S, M and L respectively after the underline of P*x*C*y* as P*x*C*y*_S, P*x*C*y*_M and P*x*C*y*_L respectively.

2.2 Characterization of scaffolds

The fibrous nanostructure and the cell morphology were observed by scanning electron microscope (SEM, S-2400, Hitachi, Japan) operating at 15 kV and 8 kV respectively. Both isotropic and aligned nanofibers diameter (average and standard deviation) were calculated from over 20 selected points in the SEM images. For cell morphology observation, the fibrous scaffolds with seeded cells were washed by phosphate buffered saline (PBS, GibcoTM, Invitrogen, USA) for 3 times and fixed by using 200 μl 4% (w/v) paraformaldehyde solution (Merck, Germany) for 30 minutes at room temperature. The cells were again washed by PBS for 3 times and subsequently freeze dehydrated.

Regarding the mechanical properties, tensile test was performed by utilizing a Criterion 42.503 (MTS) equipped with a 250 N load cell. The fibrous scaffolds were cut into a rectangular shape (10 mm in wide, 60 mm in length, and 60 μm in thickness) and tested under ambient conditions (at crosshead speed of 5 mm min^{-1}) until break. The average values and the standard deviations of mechanical parameters were calculated from five independently tests.

2.3 *In vitro* cell culture and MTT assay

H9C2 rat cardiac myoblasts were cultured in 10 cm dishes with 10 ml Dulbecco's modified Eagle's medium (DMEM, GibcoTM, Invitrogen, USA) containing 4.5 g l^{-1} glucose, 10% FBS (GibcoTM, Invitrogen, USA) and 1% penicillin/streptomycin (GibcoTM, Invitrogen, USA). Cell culture incubator was set in a condition of 5% CO_2 and 37 °C.

The fibrous scaffolds were detached from aluminum sheets, circular samples (15 mm in diameter) were cut from fibrous scaffolds and placed in 24-well tissue culture polystyrene plates (TCPS, Corning, USA). A Teflon O-ring was placed on the fibrous scaffold to prevent the scaffold from floating. All fibrous scaffolds and Teflon rings were sterilized in 70% alcohol, irradiated with the ultraviolet light overnight and then rinsed extensively with PBS. Subsequently, 1 ml of medium containing cell suspension at a density of 3×10^4 cells per ml was added to each well and maintained in a humidified atmosphere with 5% CO_2 at 37 °C. In the control group, cells cultured at the same density were also placed in empty TCPS plates and kept under the same conditions as the experimental groups (cells on fibrous scaffolds). The cell activities in both control groups and

experimental groups were tested by MTT ((3-(4,5-dimethylthiazol-2-yl)-2,5-diphenyltetrazolium bromide, a yellow tetrazole), Sigma, USA) colorimetric method. The MTT reagent was prepared as a 5 mg ml^{-1} stock solution in PBS, sterilized by Millipore filtration and kept in darkness. After culturing period, the culturing medium was removed followed by adding 200 μl MTT reagent in each well and incubated at 37 °C for 3 hours. Afterwards, the MTT reagent was replaced by 200 μl dimethyl sulfoxide (DMSO, Acros) and put on an orbital shaker (OS701, KS, Taiwan) for 15 minutes to dissolve the purple formazan crystals. The optical density at 570 nm of the purple solution was characterized by using an ELISA plate reader (ELx 800, BIO-TEK, Winooski, VT, USA). For the statistical analysis, statistical significances were calculated by employing the one-way analysis of variance in Student's *t*-test. The acceptably significant difference was determined at p value less than 0.05 (*) and 0.001 (**).

2.4 Immunocytochemistry

Identification the cytoskeletal phenotype and gap junction of cells was achieved by immunocytochemistry. After culturing for 4 days, the cells were fixed in 4% (w/v) paraformaldehyde and 0.1% Triton X-100 (Sigma) in PBS for 30 minutes. The samples were then rinsed with PBS five times and blocked with 100 μl 5% nonfat milk for 30 minutes. The primary antibodies used in this study were rabbit polyclonal antibody α-actin (diluted 1 : 25; Cell signaling, USA) and rabbit polyclonal antibody connexin-43 (diluted 1 : 75; Cell signaling, USA). Goat anti-rabbit IgG (DyLight 594) secondary antibody (diluted 1 : 50; abcam, USA), used to visualize the signal, was allowed to react with the cells for 2 hours at room temperature. Cells were also counterstained with DAPI. Immunostained cells were visualized by indirect fluorescence under a fluorescence microscope (Zeiss Axiovert 200M).

3 Results and discussion

3.1 Fibrous nanostructure of PU/EC scaffolds

The fiber diameter of the PU/EC scaffolds significantly affects the cell retention, cell proliferation and mechanical properties (discuss later) and can be simply controlled by the electrospinning processing. Herein we demonstrate the relation between the fiber diameters (D) of the developed scaffolds and processing parameters in terms of solution concentration, flow rate (Q) and applied voltage (V) during electrospinning. We employed the representative sample with blending ratio of PU/EC = 1/1 and an analytical model presented by Fridrikh *et al.* as:[36]

$$D = \left[\gamma\varepsilon\frac{I^2}{Q^2}\frac{2}{\pi(2\ln\chi - 3)}\right]^{1/3} \quad (1)$$

where γ is the surface tension of the solution, ε is the dielectric permittivity, I is the electric current and χ is the dimensionless term responsible for the normal displacements. With modification, the relation can be expressed as:

$$\log D = C_1 \log\left(\frac{Q}{V}\right) + \log C_2 \quad (2)$$

where C_1 is the constant term and C_2 is related to the terms of χ, γ and ε. Fig. 1 plots of the fiber diameters (D) verse the flow rate divided by applied voltage (Q/V) with respective to various solution concentrations. Note that the average nanofiber diameters of the scaffolds were calculated from over 20 measured widths in the SEM images. It could be seen that the plots linear relation in log scale and implied that by increasing the solution concentration, flow rate, or decreasing the applied voltage the nanofibers were getting thicker. The result was consistent with the analytical eqn (2), and the relation could be served as the guide of processing design for obtaining PU/EC scaffolds with desired nanofiber diameter. Accordingly, we fabricated scaffolds with controlled nanofiber diameters of ~100 nm, ~500 nm and ~1000 nm named for S, M and L-series.

Similarly, we were also able to control the nanofiber diameter of the scaffolds in the other two blending ratio, *i.e.* PU/EC = 4/1 and PU/EC = 9/1, which were denoted as P4C1_S, P4C1_M, P4C1_L, and P9C1_S, P9C1_M, P9C1_L respectively. The SEM images of the P1C1_S, P1C1_M, and P1C1_L scaffolds were representatively shown in Fig. 2 accompanied by the scaffold fabricated from pristine PU for comparison. It could be observed that the PU scaffolds (Fig. 2a) reveal intertwining (and clinginess) between the fibers while the PU/EC scaffolds (Fig. 2b–d) showed more uniform and smoother nanofibers in three dimensional webs. The results implied that blending EC into PU could improve the processability of scaffolds with uniform fibrous and porous nanostructures. The interconnected porosity and large surface-area to volume ratio of PU/EC scaffolds would assist in nutrition perfusion and diffusion. Furthermore, the nanofibers with uniform diameter would also facilitate the cell adhesion.

3.2 Biocompatibility of PU/EC scaffolds

The biocompatibility of the developed scaffolds was investigated for potential application of *in vitro* cardiac tissue

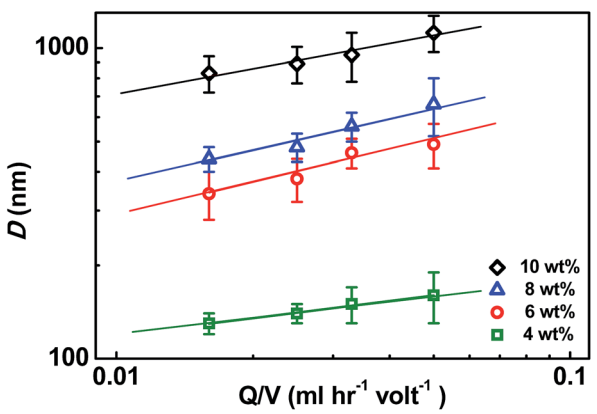

Fig. 1 Plots of the relation between nanofiber diameter (D) and flow rate divide by applied voltage (Q/V) with respective to various concentrations of polymer blending solutions, *i.e.* 4 wt%, 6 wt%, 8 wt% and 10 wt%. The samples are with polymer blending ratio of PU/EC = 1/1, *i.e.* P1C1.

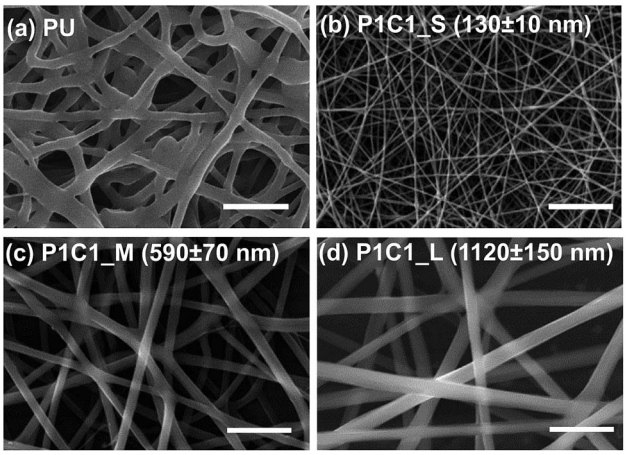

Fig. 2 SEM images of PU and PU/EC scaffolds with blending ratio of PU/EC = 1/1 with various nanofiber diameters, *i.e.* (a) PU, (b) P1C1_S, (c) P1C1_M, and (d) P1C1_L. The average diameters and standard deviations were calculated from over 20 measured widths of the nanofibers in the SEM images. The scale bar is 50 μm in length.

engineering. To investigate the change of pH value caused by scaffolds, we immersed scaffolds (taking the P1C1_M and pristine PU for examples) into phosphate buffer saline for 20 weeks and recorded at intervals. The steady pH value were shown in Fig. 3a as around 7.5–7.6 which implies that the developed scaffolds in the present work would not generate substances which affect the pH value and deteriorate cell proliferation.

The cell viability MTT assay was carried out to analyze the cardiac myoblast H9C2 cell populations after being cultured on different scaffolds for 4 hours, 1 day, 4 days and 7 days

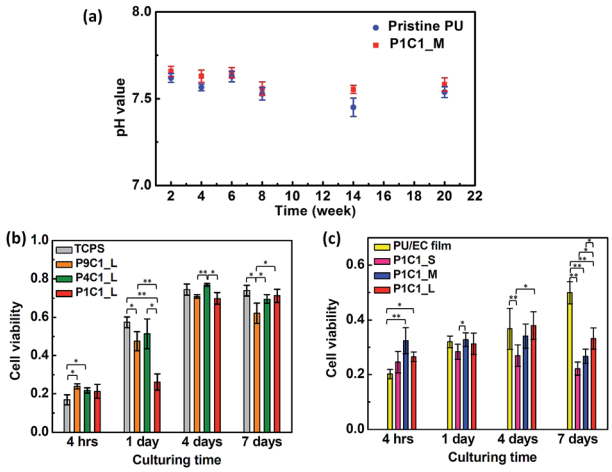

Fig. 3 (a) pH values of pristine PU and P1C1_M scaffolds being immersed into phosphate buffer saline within 22 weeks. (b) Growth of H9C2 cells on scaffolds with nanofiber diameter around 1000 nm with respective to different PU/EC blending ratios, *i.e.* P1C1_L, P4C1_L, and P9C1_L. (c) Growth of H9C2 cells on PU/EC scaffolds (blending ratio of 1/1) with different diameters, *i.e.* P1C1_S, P1C1_M and P1C1_L. The cell growth performed on the control samples of TCPS and PU/EC film (without nanostructure) are also shown.

respectively. We studied the effects of two different parameters on the biocompatibility of scaffolds. The first one was PU/EC blending ratios (*i.e.* P9C1_L, P4C1_L and P1C1_L) and the second one was diameters of nanofibers (*i.e.* P1C1_S, P1C1_M and P1C1_L). The results were presented in Fig. 3b and c respectively. The average cell populations with various cultured time were indicated by the optical density (O. D.) of the purple solution (with dissolved purple formazan crystals) at wavelength of 570 nm (*cf.* methods section). From Fig. 3b we found that cells seeded on P9C1_L, P4C1_L and P1C1_L scaffolds all showed increasing populations over the culturing time for 4 days and remained stable to 7 days, which were similar to the trends of cells growing on TCPS. The O. D. values of three scaffolds on day 7 were three times higher than those of 4 hours, suggesting that our developed PU/EC scaffolds possessed certain biocompatibility that enables the cell retention and proliferation over the time frame in this study. Regarding the effects of fiber diameters on cell growth, we studied the cell activities on three kinds of scaffolds including P1C1_S, P1C1_M and P1C1_L for one week. A thin film (without nanostructures) casted from PU/EC polymer blending solution with ratio of 1/1 was also performed for comparison. It was interesting to find that at the beginning of 4 hours, cell populations were higher on fibrous scaffolds than on the smooth substrate (Fig. 3b, c and 7), which implied that fibrous structure provides more recognition sites for cell adhesion. Additionally, from Fig. 3c, P1C1_L remarkably showed higher cell activity than those of P1C1_S and P1C1_M. The higher biocompatibility of P1C1_L could be attributed due to the larger interconnected pores for nutrition and waste exchange. The results suggested that for the application of PU/EC scaffolds, certain thickness (~1000 nm) of nanofibers should be obtained for supporting cell viability.

The cell morphologies (cultured for 4 hours) on different substrates were shown in Fig. 4. The cells seeded on P1C1_S and P1C1_M scaffolds were stretched out strip-like filopodia, while cells seeded on P1C1_L scaffolds, PU/EC film and TCPS were stretched out two-dimensional projections called lamellipodium. Filopodia and lamellipodium are both cytoplasmic projections composed of actin filaments cross-linked into bundles or meshes. Many types of migrating cells display filopodia which have roles in cell–cell interactions, sensation of

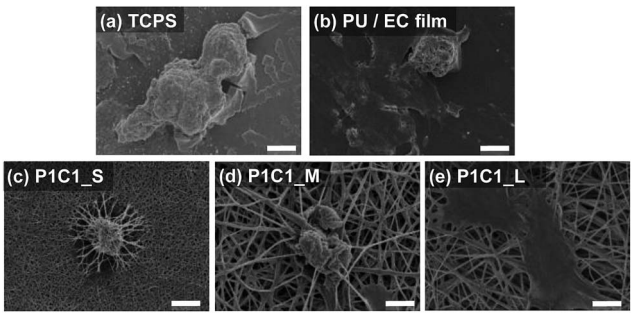

Fig. 4 SEM images of (a) TCPS, (b) PU/EC film and (c–e) PU/EC scaffolds (ratio of 1/1) with different nanofiber diameters, (c) P1C1_S, (d) P1C1_M, and (e) P1C1_L after cell culturing for 4 hours. The scale bar is 10 μm in length.

chemical cues and changes in directed motion. For the lamellipodium, they are believed to be the actual motor pulling cells forward during cell migration. The morphological observation supported the results of MTT assay analysis, *i.e.* the PU/EC scaffolds with thicker nanofibers exhibits higher cell activities than those with thinner nanofibers.

3.3 Mechanical properties of PU/EC scaffolds

Proper mechanical properties of the developed PU/EC blending scaffolds are crucial in potential application of cardiac tissue engineering and were investigated. In short, the scaffolds should possess sufficient mechanical strength/stiffness (*e.g.* Young's modules, tensile strength, *etc.*) to support the force produced by myocardial tissue during constant cyclic deformation of heart beating. Additionally, criteria of ductile/elasticity should be met for flexibly accommodating the contractile tissues. Herein, owing to the weak biocompatibility of S-series scaffolds, we focused on investigating M- and L-series scaffolds with respective to different blending ratios, *i.e.* P1C1_M, P1C1_L, P4C1_M, P4C1_L, P9C1_M, and P9C1_L in the following section. The pristine PU scaffolds (with nanofiber diameter around 500 nm) were also analyzed for comparison. The mechanical properties (Young's modulus, tensile strength and elongations at break) extracted from the stress–strain tests were summarized in Table 1 and the representative stress–strain curves were shown in Fig. 5a.

The average values and the standard deviations were calculated from five independently tests for each sample condition. Generally, by increasing the blending concentration of EC in PU, the Young's modulus was increased and elongation at break was decreased, which were the consequences of the intrinsic properties of respective materials. It was interesting to find out that blending small amount of EC (P9C1_M and P9C1_L) leads to significantly increased tensile strength as compared with pristine PU. However, tensile strength was declined after further increasing the blending concentration of EC (*i.e.* P1C1_M and P1C1_L), which also induced high Young's modules and low elongation at break. Such brittle characteristics are not suitable for tissue engineering application.

Regarding the scaffolds with different nanofiber diameters, higher Young's modulus and tensile strength but lower elongation was found in scaffolds with thinner nanofibers. It could

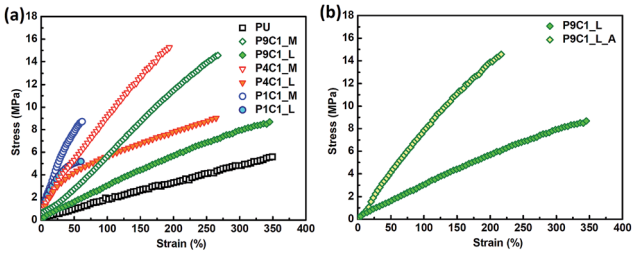

Fig. 5 (a) Stress–strain curves of pristine PU scaffolds and PU/EC scaffolds with different nanofiber diameters with respect to different blending ratios, *i.e.* P9C1_M, P9C1_L, P4C1_M, P4C1_L, P1C1_M, and P1C1_L. (b) Stress–strain curves of PU/EC (ratio of 9/1) scaffolds with isotropic and aligned nanofibers (~1000 nm), *i.e.* P9C1_L and P9C1_L_A respectively.

be attributed to the different polymer conformation in the nanofibers, namely, during the electrospinning the thinner nanofibers experienced stronger drawing effect which leads to higher crystallinity and partially aligned amorphous polymer chains along nanofiber axis.[37] Additionally, from the obtained mechanical parameters the PU/EC scaffolds showed significant higher mechanical strength (*e.g.* Young's modulus around 1–90 MPa) than that of the cardiac tissue. This enabled the fabrication, processing and handling of ultra-thin scaffolds patch (tens or hundreds of micrometer) which facilitates the cell delivery for therapeutic purposes. Furthermore, the high elongation (tens or hundreds of percent) imparts the elastomeric characteristics suggests that the ultra-thin scaffolds are still flexibly compliant with the contractile cardiac muscle.

3.4 PU/EC scaffolds with aligned nanofibers

Material with anisotropic property is the central goal of developing bioengineered scaffolds for structurally mimicking the extracellular matrix of cardiac tissue, guiding the orientation of cardiac myoblasts with native anisotropy, and furthermore promoting the directional function of the heart contraction and heart communication (*e.g.* propagation of electrical signals). In order to achieve this goal using the developed PU/EC scaffolds, herein we used a rotating collector during electrospinning to obtain PU/EC scaffolds (taking blending ratio of PU/EC = 9/1 for example) with aligned nanofibers (denoted as P9C1_L_A).

Table 1 Summary of mechanical properties of pristine PU scaffolds and PU/EC scaffolds with different nanofiber diameters with respective to different blending ratios, *i.e.* P9C1_M, P9C1_L, P4C1_M, P4C1_L, P1C1_M, and P1C1_L. The mechanical properties of PU/EC (9/1 ratio) scaffold with aligned nanofibers (P9C1_L_A) are also shown

Samples	Young's modulus (MPa)	Tensile strength (MPa)	Elongation (%)
PU	1.5 ± 0.20	4.6 ± 1.08	286.2 ± 62.40
P9C1_M	3.6 ± 0.55	12.8 ± 3.27	213.8 ± 39.19
P9C1_L	2.9 ± 0.01	8.1 ± 0.67	329.0 ± 19.44
P4C1_M	8.4 ± 1.38	11.6 ± 2.77	160.4 ± 23.72
P4C1_L	7.2 ± 2.70	6.3 ± 1.64	294.1 ± 54.65
P1C1_M	87.2 ± 12.35	7.6 ± 3.51	47.3 ± 6.47
P1C1_L	51.3 ± 11.53	4.8 ± 0.52	45.1 ± 16.10
P9C1_L_A	4.5 ± 1.21	12.3 ± 3.47	230.1 ± 18.11

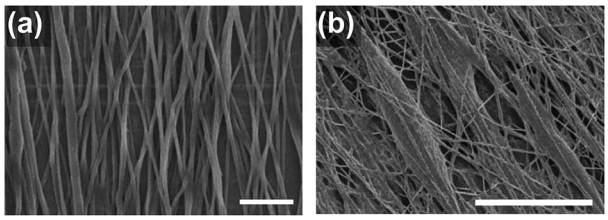

Fig. 6 (a) SEM image of PU/EC scaffold (ratio of 9/1) with aligned nanofibers, *i.e.* P9C1_L_A. (b) SEM image of P9C1_L_A scaffold after H9C2 cells cultured for 4 h. The scale bar is 100 μm in length.

Fig. 6a showed the SEM image of P1C1_L_A scaffolds reveal successfully aligned nanofibers with diameter of 1190 nm ± 210 nm. The similar test of biocompatibility by culturing H9C2 cell and using MTT assay were performed on P1C1_L_A scaffolds.

From Fig. 7, a significant higher cell population was found on P9C1_L_A scaffolds than on P9C1_L after culturing for 4 days and 7 days. Additionally, the P9C1_L_A scaffolds showed the same growth rate with TCPS. These results indicated that the aligned fibrous structure possess as good biocompatibility as TCPS does. It is noteworthy that both P9C1_L and TCPS show little different trend of cell growth during the timeframe from day 4 to day 7 as compared to the resulted shown in Fig. 3. This discrepancy can be attributed to the experimental errors since they were performed in two different batches. Such deviation errors can be resulted from the lack of nutrition and/or space for cell growth, which is typically significant for long time culturing. However, such error does not affect the interpretation of biocompatibility of the scaffolds in the present study. In addition, cells on P9C1_L_A scaffolds were found to be organized and oriented toward the aligned nanofibers with spindle morphology (Fig. 6b), which were very distinct from the flat morphologies of cells spread on isotropic scaffolds (*cf.* Fig. 4e). The organization of cells indicated that the aligned nanofibers could functionally provide topographic cues for cell alignment. The strong adoption of cells on anisotropic fibrous nanostructures mimicked the *in vivo* cardiac anisotropy and would help the cell adhesion, proliferation and even more differentiation for potentially guiding cardiac reconstruction and tissue establishment.

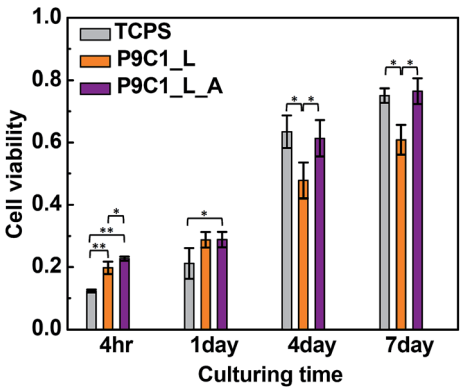

Fig. 7 Growth of H9C2 cells on isotropic and aligned scaffolds with PU/EC blending ratio of 9/1 and nanofiber diameter around 1000 nm, *i.e.* P9C1_L and P9C1_L_A respectively.

The cell morphology/function on engineered scaffolds of P9C1_L and P9C1_L_A could be furthermore evaluated by phenotypic protein of cardiac myoblast expressions. After 4 days cultured, the α-actin (muscle-specific intermediate filament protein) and connexin 43 (constituent of cardiomyocyte gap junction) were examined by immunofluorescence staining as shown in Fig. 8. The electrical communication between cardiomyocytes is mediated by connexin 43 which is the most prominent gap junction proteins.[13,33] From the fluorescent figures of staining for α-actin, the cells on isotropic scaffolds (P9C1_L) were less spreading and isolated on the fibrous matrices. In contrast, the cells cultured on aligned fibrous P9C1_L_A were more populated and spreading with nuclei surround by mature cytoskeleton. Moreover, the cells revealed more directionally arranged (indicated by white arrow) and extended phenotype with tighter intercellular contacts. However, note that for the connexin 43 staining the gap junctions were found around the nuclei without clear end-to-end cell coupling in both scaffolds. Such observation was similar to the phenotype observed by Rockwood *et al.*[33] Fig. 8j shows the intensity plot of connexin-43. The high intensity for TCPS indicates a high amount of cell–cell contact. However, the intensity for P9C1_L and P9C1_LA are much lower than TCPS,

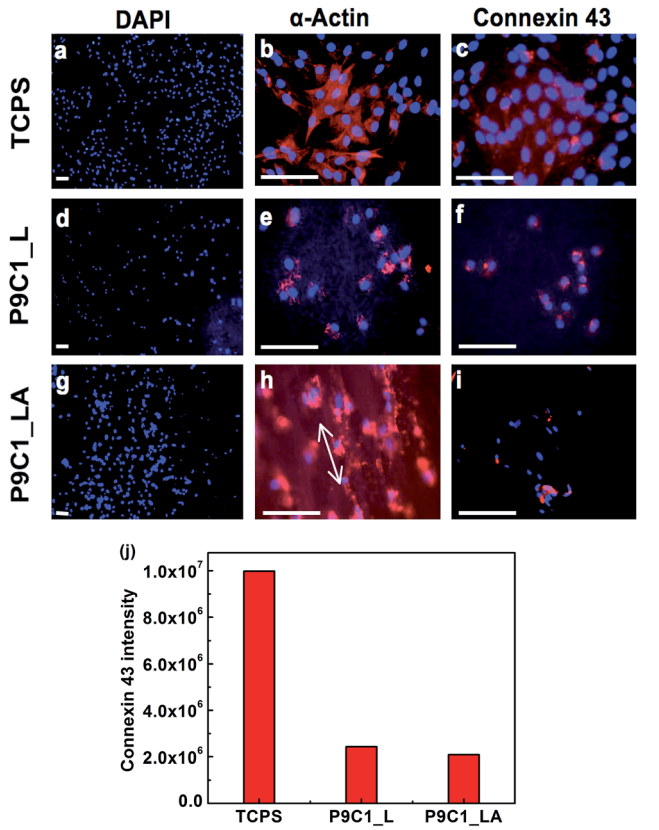

Fig. 8 Immunofluorescent microscopic images of H9C2 morphologies after seeded on (a–c) TCPS, (d–f) isotropic fibrous scaffolds P9C1_L and (g–i) anisotropic fibrous scaffolds P9C1_L_A. The samples were stained for nuclei (blue), α-actin (red in b, e and h) and gap-junction-specific connexin-43 (red in c, f and i). (j) Connexin 43 intensity. The scale bar is 100 μm in length.

which we attribute to the three dimensional (3D) nanostructure of the fibrous scaffolds in contrast to the planar TCPS substrate. Specifically, according to the cell viability data shown in Fig. 7, the cell population for TCPS and P9C1_LA are nearly the same which suggests that they should have similar amount of cell–cell contact. However, while the cells lying on the planar TCPS substrates are easy of staining, it would be relatively difficult to stain all of the cells growing inside the fibrous scaffold because of the 3D spaces. Additionally, it's also difficult to focus camera on cells that stay in different depth. In short conclusion, the results of immunofluorescence indicated the cells adopted the anisotropic fibrous nanostructures. They mimicked the *in vivo* cardiac anisotropy that would be helpful in cell adhesion and proliferation for potential cardiac reconstruction.

The mechanical properties of the P9C1_L_A scaffolds would be of interesting owing to its unique nanostructure. Fig. 5b plotted the representative stress–strain curves of P9C1_L and P9C1_L_A scaffolds and the mechanical parameters are summarized in Table 1 (with average and standard deviation calculated from 5 independently performed tests for each sample). The P9C1_L_A scaffolds possessed stronger mechanical strength with higher Young's modulus (4.5 MPa), higher tensile strength (12.3 MPa) but lower elongation (230.1%) as compared with P9C1_L scaffolds. The reinforced mechanical strength of P9C1_L_A scaffolds could be attributed to larger amount of nanofibers per stress-loaded area along the directionally aligned bundles. The enhanced stiffness was accompanied by declined elongation since the aligned nanofibers were less extendable; however, the elongation was still much larger than those of cardiac muscle which retain the mechanical compatibility and potential synchronous deformation in between.

4 Conclusions

In conclusion, we newly introduced an electrospun fibrous scaffold of PU/EC polymer blend, revealing uniform fiber diameter and interconnected porous nanostructures as compared to the pristine PU. We established the analytical relation between nanofiber diameters and processing conditions which could serve as the guide for fabricating PU/EC scaffolds with desired diameters. The scaffolds with thicker nanofibers were found to provide more cell recognition sites which facilitate cell retention and proliferation. The PU/EC scaffolds exhibit high mechanical strength for supporting contractile cardiac tissues but still retain elastomeric characteristics for flexibly accommodating cardiac deformation. Anisotropic PU/EC scaffolds were successfully obtained which significantly improve the cell guidance/regulation and proliferation for mimicking the extracellular matrix of myocardium. The results implied the potential in achieving therapeutic purposes by bioengineering the developed PU/EC scaffolds as a cardiac graft for reconstructing or regeneration damaged myocardium.

Acknowledgements

Financial supports for this work obtained from the National Science Council of Taiwan (NSC 101-2120-M-002-003 and NSC 102-2120-M-002-010) are highly appreciated.

References

1 Q.-Z. Chen, S. E. Harding, N. N. Ali, A. R. Lyon and A. R. Boccaccini, *Mater. Sci. Eng., R*, 2008, **59**, 1.
2 M. Perán, M. García, E. Lopez-Ruiz, G. Jiménez and J. Marchal, *Materials*, 2013, **6**, 1333.
3 R. Sui, X. Liao, X. Zhou and Q. Tan, *Stem Cell Rev.*, 2011, **7**, 172.
4 P. A. Gunatillake and R. Adhikari, *Eur. Cells Mater.*, 2003, **5**, 1.
5 T. Dvir, B. P. Timko, D. S. Kohane and R. Langer, *Nat. Nanotechnol.*, 2011, **6**, 13.
6 A. P. Nowak, V. Breedveld, L. Pakstis, B. Ozbas, D. J. Pine, D. Pochan and T. J. Deming, *Nature*, 2002, **417**, 424.
7 W.-H. Zimmermann, I. Melnychenko and T. Eschenhagen, *Biomaterials*, 2004, **25**, 1639.
8 K. L. Christman, Q. Z. Fang, M. S. Yee, K. R. Johnson, R. E. Sievers and R. J. Lee, *Biomaterials*, 2005, **26**, 1139.
9 R. K. Li, Z. Q. Jia, R. D. Weisel, D. A. G. Mickle, A. Choi and T. M. Yau, *Circulation*, 1999, **100**, 63.
10 G. C. Engelmayr, M. Y. Cheng, C. J. Bettinger, J. T. Borenstein, R. Langer and L. E. Freed, *Nat. Mater.*, 2008, **7**, 1003.
11 H. M. Nugent and E. R. Edelman, *Circ. Res.*, 2003, **92**, 1068.
12 D. Garlotta, *J. Polym. Environ.*, 2001, **9**, 63.
13 C. W. Hsiao, M. Y. Bai, Y. Chang, M. F. Chung, T. Y. Lee, C. T. Wu, B. Maiti, Z. X. Liao, R. K. Li and H. W. Sung, *Biomaterials*, 2013, **34**, 1063.
14 S. Mukherjee, C. Gualandi, M. L. Focarete, R. Ravichandran, J. R. Venugopal, M. Raghunath and S. Ramakrishna, *J. Mater. Sci.: Mater. Med.*, 2011, **22**, 1689.
15 M. P. Prabhakaran, A. S. Nair, D. Kai and S. Ramakrishna, *Biopolymers*, 2012, **97**, 529.
16 P. Balasubramanian, M. P. Prabhakaran, D. Kai and S. Ramakrishna, *J. Biomater. Sci., Polym. Ed.*, 2013, **24**, 1660.
17 A. D'Amore, J. A. Stella, W. R. Wagner and M. S. Sacks, *Biomaterials*, 2010, **31**, 5345.
18 J. D. Fromstein, P. W. Zandstra, C. Alperin, D. Rockwood, J. F. Rabolt and K. A. Woodhouse, *Tissue Eng., Part A*, 2008, **14**, 369.
19 M. K. Gupta, J. M. Walthall, R. Venkataraman, S. W. Crowder, D. K. Jung, S. S. Yu, T. K. Feaster, X. Wang, T. D. Giorgio, C. C. Hong, F. J. Baudenbacher, A. K. Hatzopoulos and H.-J. Sung, *PLoS One*, 2011, **6**, e28935.
20 Q. P. Pham, U. Sharma and A. G. Mikos, *Tissue Eng.*, 2006, **12**, 1197.
21 M. Shin, O. Ishii, T. Sueda and J. P. Vacanti, *Biomaterials*, 2004, **25**, 3717.
22 P. R. Sreerekha, D. Menon, S. V. Nair and K. P. Chennazhi, *Tissue Eng., Part A*, 2013, **19**, 849.

23 T. Courtney, M. S. Sacks, J. Stankus, J. Guan and W. R. Wagner, *Biomaterials*, 2006, **27**, 3631.
24 D. Kai, M. P. Prabhakaran, G. Jin and S. Ramakrishna, *J. Biomed. Mater. Res., Part B*, 2011, **98**, 379.
25 J. Guan, F. Wang, Z. Li, J. Chen, X. Guo, J. Liao and N. I. Moldovan, *Biomaterials*, 2011, **32**, 5568.
26 I. C. Parrag, P. W. Zandstra and K. A. Woodhouse, *Biotechnol. Bioeng.*, 2012, **109**, 813.
27 X. Zong, H. Bien, C. Y. Chung, L. Yin, D. Fang, B. S. Hsiao, B. Chu and E. Entcheva, *Biomaterials*, 2005, **26**, 5330.
28 C. Alperin, P. W. Zandstra and K. A. Woodhouse, *Biomaterials*, 2005, **26**, 7377.
29 T. C. McDevitt, K. A. Woodhouse, S. D. Hauschka, C. E. Murry and P. S. Stayton, *J. Biomed. Mater. Res. A.*, 2003, **66**, 586.
30 K. L. Fujimoto, K. Tobita, W. D. Merryman, J. Guan, N. Momoi, D. B. Stolz, M. S. Sacks, B. B. Keller and W. R. Wagner, *J. Am. Coll. Cardiol.*, 2007, **49**, 2292.
31 M. N. Giraud, R. Flueckiger, S. Cook, E. Ayuni, M. Siepe, T. Carrel and H. Tevaearai, *Artif. Organs*, 2010, **34**, E184.
32 P. A. Nair and P. Ramesh, *J. Biomed. Mater. Res. A.*, 2013, **101**, 1876.
33 D. N. Rockwood, R. E. Akins Jr, I. C. Parrag, K. A. Woodhouse and J. F. Rabolt, *Biomaterials*, 2008, **29**, 4783.
34 M. Siepe, M. N. Giraud, E. Liljensten, U. Nydegger, P. Menasche, T. Carrel and H. T. Tevaearai, *Artif. Organs*, 2007, **31**, 425.
35 J. J. Stankus, J. Guan, K. Fujimoto and W. R. Wagner, *Biomaterials*, 2006, **27**, 735.
36 S. Fridrikh, J. Yu, M. Brenner and G. Rutledge, *Phys. Rev. Lett.*, 2003, **90**, 144502.
37 S. C. Wong, A. Baji and S. W. Leng, *Polymer*, 2008, **49**, 4713.